

See discussions, stats, and author profiles for this publication at: <https://www.researchgate.net/publication/229080129>

Effects of the Pathological Q212P Mutation on Human Prion Protein Non-Octarepeat Copper-Binding Site

ARTICLE in **BIOCHEMISTRY** · JULY 2012

Impact Factor: 3.02 · DOI: 10.1021/bi300233n · Source: PubMed

CITATIONS

11

READS

45

9 AUTHORS, INCLUDING:



[Alessandro Arcovito](#)

Catholic University of the Sacred Heart

70 PUBLICATIONS 1,047 CITATIONS

[SEE PROFILE](#)



[Giovanni Chillemi](#)

Cineca

104 PUBLICATIONS 1,726 CITATIONS

[SEE PROFILE](#)



[Gabriele Giachin](#)

European Synchrotron Radiation Facility

27 PUBLICATIONS 226 CITATIONS

[SEE PROFILE](#)



[Federico Benetti](#)

Scuola Internazionale Superiore di Studi Avan...

37 PUBLICATIONS 207 CITATIONS

[SEE PROFILE](#)

Effects of the Pathological Q212P Mutation on Human Prion Protein Non-Octarepeat Copper-Binding Site

Paola D'Angelo,^{*,†} Stefano Della Longa,[‡] Alessandro Arcovito,[§] Giordano Mancini,^{||} Andrea Zitolo,[†] Giovanni Chillemi,^{||} Gabriele Giachin,[‡] Giuseppe Legname,^{*,‡,○} and Federico Benetti^{*,‡,§,▽}

[†]Department of Chemistry, University of Rome “La Sapienza”, P.le Aldo Moro 5, I-00185 Rome, Italy

[‡]Dipartimento di Medicina Clinica, Sanità Pubblica, Scienze della Vita e dell'Ambiente, Università dell'Aquila, I- 67100 L'Aquila, Italy

[§]Istituto di Biochimica e Biochimica Clinica, Università Cattolica del Sacro Cuore, L.go F. Vito 1, I-00168 Rome, Italy

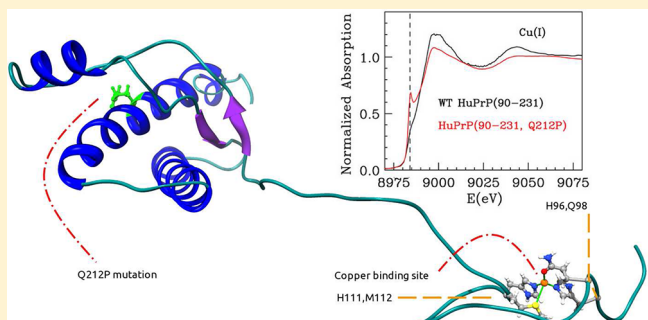
^{||}CASPUR, Consortium for Supercomputing Applications, Via dei Tizii 6b, I-00185 Rome, Italy

[○]Laboratory of Prion Biology, Department of Neuroscience, Scuola Internazionale Superiore di Studi Avanzati (SISSA), Via Bonomea 265, I-34136 Trieste, Italy

^{*}SISSA Unit, Italian Institute of Technology, Via Bonomea 265, I-34136 Trieste, Italy

[○]ELETTRA Laboratory, Sincrotrone Trieste S.C.p.A., I-34149, Basovizza, Trieste, ITALY

ABSTRACT: Prion diseases are a class of fatal neurodegenerative disorders characterized by brain spongiosis, synaptic degeneration, microglia and astrocytes activation, neuronal loss and altered redox control. These maladies can be sporadic, iatrogenic and genetic. The etiological agent is the prion, a misfolded form of the cellular prion protein, PrP^C. PrP^C interacts with metal ions, in particular copper and zinc, through the octarepeat and non-octarepeat binding sites. The physiological implication of this interaction is still unclear, as is the role of metals in the conversion. Since prion diseases present metal dyshomeostasis and increased oxidative stress, we described the copper-binding site located in the human C-terminal domain of PrP–HuPrP(90–231), both in the wild-type protein and in the protein carrying the pathological mutation Q212P. We used the synchrotron-based X-ray absorption fine structure technique to study the Cu(II) and Cu(I) coordination geometries in the mutant, and we compared them with those obtained using the wild-type protein. By analyzing the extended X-ray absorption fine structure and the X-ray absorption near-edge structure, we highlighted changes in copper coordination induced by the point mutation Q212P in both oxidation states. While in the wild-type protein the copper-binding site has the same structure for both Cu(II) and Cu(I), in the mutant the coordination site changes drastically from the oxidized to the reduced form of the copper ion. Copper-binding sites in the mutant resemble those obtained using peptides, confirming the loss of short- and long-range interactions. These changes probably cause alterations in copper homeostasis and, consequently, in redox control.



The cellular form of the prion protein (PrP), PrP^C, is linked to the outer leaflet of plasma membrane through a glycosylphosphatidylinositol anchor. It is expressed mostly in the central and peripheral nervous systems. The NMR structures of recombinant human PrP (HuPrP) revealed a flexibly disordered N-terminal domain and a globular domain encompassing residues 125–228.¹ The globular domain contains three α -helices (spanning residues 144–154, 173–194 and 200–228) and two short β -strands (128–131 and 161–164). The C-terminal domain has a disulfide bridge, connecting cysteines 179 and 214, and two N-linked carbohydrates at asparagines 181 and 197. Residues 51–91 consist of unusual glycine-rich repeats. Residues 60–91 form four octarepeat regions (OR) PHGGW_nQ, while residues 51–59 form a nonapeptide, which lacks the histidine residue (PQGGGTWGQ). This region is highly conserved among

mammals. The OR segment binds copper and other divalent cations such as zinc, nickel, iron and manganese.^{2–8} This segment has highest affinity for copper ions, sensing to specific concentrations of the metal by transitioning from a multi-His binding mode at low copper levels to a single-His, amide nitrogen mode at high copper levels.^{9,10} Moreover, this region binds four copper ions cooperatively with micromolar affinity around 5–8 μ M.^{11,12} Additional histidines, at positions 96 and 111, are involved in high affinity (i.e., 10^{-14} M) copper-binding site formation (Figure 1).^{6,13–15} This segment is referred to as the non-OR copper-binding site. Both OR-copper (high occupancy) and non-OR-copper complexes sustain Cu(II)

Received: February 20, 2012

Revised: June 20, 2012

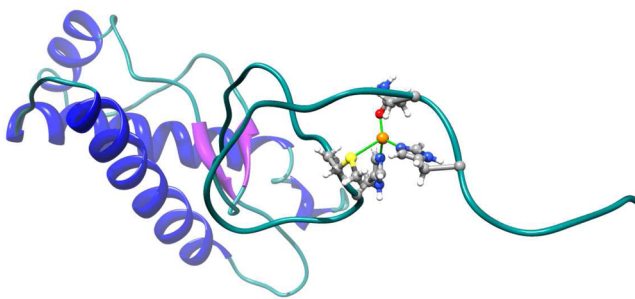


Figure 1. Schematic representation of the copper–HuPrP(90-231) complex. Blue indicates the three α -helices, purple the two β -strands and cyan the unfolded N-terminal part of the globular domain.

redox cycling. The inability of O_2 to oxidize OR–Cu(I) halts the Cu(II) redox cycling.¹⁰ Although many studies have been carried out to elucidate the role of PrP^C–metal complexes *in vitro*, their role and functioning *in vivo* are still unclear.

The widely expressed PrP^C plays a role in many physiological functions, such as neuroprotection against apoptosis and oxidative stress,^{16,17} neurite outgrowth,^{18–20} maintenance of myelinated axons,²¹ copper homeostasis^{22–24} and synapse formation and function.²¹ Mice lacking PrP^C are more susceptible to oxidative damage to proteins and lipids.^{16,25}

PrP^C can be converted into its pathological form denoted as prion or PrP^{Sc}. This represents the etiological agent of prion diseases or transmissible spongiform encephalopathies (TSEs).²⁶ These disorders are characterized by spongiform neurodegeneration of the central nervous system and include Creutzfeldt–Jakob disease, Gerstmann–Sträussler–Scheinker (GSS) syndrome, fatal familial insomnia and kuru in humans; bovine spongiform encephalopathy in cattle; scrapie in sheep and goats; and chronic wasting disease in elk, deer and moose.²⁷ PrP^{Sc} and its physiological counterpart, PrP^C, share a common sequence and pattern of post-translational modifications, but they possess different secondary and tertiary structures and physicochemical properties.^{26,28,29} The infectious PrP^{Sc} is distinguished from PrP^C by its resistance to protease digestion in nondenaturing conditions. Limited proteolysis and antibody labeling identified the C-terminal domain as the region involved in the conversion.³⁰ After hydrolysis, PK-resistant PrP^{Sc} appears as a truncated form, lacking its N-terminal region.³¹ The PK-resistant core retains infectivity.

Prion diseases can be genetic, acquired or sporadic. The familial forms are due both to nonsynonymous point mutations occurring in the PrP gene (*PRNP* in humans) and to insertions or deletions of the OR.³² Currently, over 55 mutations in the *PRNP* gene are known. Mutations may destabilize PrP^C thermodynamically,^{33–36} escape quality control cellular pathway and accumulate inside the cell,^{37–40} as well as alter surface properties favoring aberrant interactions with physiological interactors. Spectroscopic and molecular dynamics studies have shown that point mutations clustered in the globular domain may alter both short- and long-range interactions.^{41–44} For example, Yin and colleagues⁴⁴ outlined the effects of pathological point mutations in the binding of PrP with glycosaminoglycan (GAG).⁴⁴ The investigated point mutations, located in the globular domain, caused the exposure to the solvent of the normally buried 109–136 region, thus altering GAG binding.

To date many efforts have been made to highlight the effect of pathological point mutations on PrP tertiary structure. As TSEs are also characterized by metal dys-homeostasis and increased oxidative stress,⁴⁵ we investigated the effect of mutations on the non-OR copper-binding site. This is located in the highly fibrillogenic and toxic region PrP106–126, and divalent cations have been shown to modulate protein aggregation and neurotoxic properties.^{46,47} Here, we describe the copper-binding site located in the human C-terminal domain of PrP–HuPrP(90-231), carrying the pathological mutation Q212P. This mutation is responsible for a rare GSS syndrome characterized by mild amyloid PrP deposition in patients.^{48,49} Q212P mutant represents a unique case in prion structural biology in which a mutation induces remarkable structural differences, including disruption of the C-terminal part of the α_3 helix, solvent exposure of hydrophobic residues and a different orientation of α_2 and α_3 helices.⁴¹ For these reasons this mutant may represent a good model to evaluate critical epitopes of PrP involved in the conversion process. Because of the redox cycling of the non-OR copper-binding site, we used the synchrotron-based X-ray absorption fine structure (XAFS) technique to study Cu(II) and Cu(I) coordination geometries in the mutant, and compared them with those obtained using wild-type (WT). XAFS spectroscopy is a powerful tool to investigate both local structure and dynamics on a wide class of metal-containing proteins.^{50–53} This technique is very sensitive to the coordination geometry of an absorbing atom and thus allows the measurement of bond distances and angles of the surrounding atomic cluster with atomic resolution. XAFS focuses on either the extended X-ray absorption fine structure (EXAFS)⁵⁴ or the X-ray absorption near-edge structure (XANES).^{55,56} Comparison of XANES and EXAFS spectra of WT and Q212P mutant PrP highlighted modifications of the copper-binding site induced by the pathological point mutation. It also provided new insights into the early events of conformational transition of PrP^C into PrP^{Sc} and the role of copper in this process.

MATERIALS AND METHODS

Plasmid Construction. The WT HuPrP(90-231, M129) was amplified from genomic human DNA by PCR using primers 5'-GGA ATT CCA TAT GGG TCA AGG AGG TGG CAC CCA C-3' and 5'-CGG GAT CCC TAG CTC GAT CCT CTC TGG TAA TAG GCC TGA-3'. The DNA product was then inserted into pET-11a vector (Novagen) using *Nde*I and *Bam*H I restriction sites. The Q212P mutant was constructed with the QuikChange kit (Stratagene) utilizing primers 5'-CGC GTG GTT GAG CCG ATG TGT ATC ACC C-3' and 5'- GGG TGA TAC ACA TCG GCT CAA CCA CGC G-3', and pET11a::HuPrP(90-231, M129) as template. The cloned DNA sequences were verified by sequencing.

Protein expression, purification and samples preparation. Freshly transformed overnight culture of *Escherichia coli* BL21 (DE3) cells (Stratagene) was added at 37 °C to 2 L of ZYM-5052 autoinduction medium⁵⁷ plus ampicillin (100 µg/mL). Cells were grown in a Biostat B plus 2 L vessel (Sartorius) and harvested 18 h after inoculation. Bacterial paste was resuspended in 25 mM Tris-HCl, 5 mM EDTA, 0.8% Triton X-100, 0.4% deoxycholic acid, 1 mM PMSF, pH 8 and lysed by French press (EmulsiFlex-C3). Inclusion bodies were separated by centrifugation (30 min, 10,000 g at 4 °C), rinsed in 25 mM Tris-HCl, 5 mM EDTA, 0.8% TritonX100, pH 8, and several times in bidistilled water. Pure inclusion bodies

were solubilized in 5 volumes of 8 M GndHCl, 100 mM DTT, pH 8 and loaded onto a size-exclusion chromatography column (Superdex 200 26/60, GE). Proteins were eluted with 6 M GndHCl, 25 mM Tris-HCl, 5 mM EDTA, pH 8 at a flow rate of 2 mL/min. Eluted proteins were stored at 4 °C for 2 weeks for oxidation. Oxidized proteins were purified by reverse-phase (Jupiter C4, 250 mm × 21.2 mm, 300 Å pore size, Phenomenex) and separated using a linear gradient of 0–90% acetonitrile, 0.1% trifluoroacetic acid. Purified proteins were analyzed by SDS-PAGE, Western blot and electrospray mass spectrometry, and then lyophilized. Refolding was performed dissolving the proteins in 8 M GndHCl and dialyzing them against 20 mM sodium acetate, pH 5.5 using a Spectrapor-membrane (MW 3000). Protein folding was analyzed by circular dichroism.

Samples with 1:1 Cu(II):HuPrP(90-231)/HuPrP(90-231, Q212P) ratio were prepared in acetate buffer. The Cu(I):HuPrP(90-231)/HuPrP(90-231, Q212P) complexes were generated reducing Cu(II) with 40 mM ascorbate. The metal:protein ratios were confirmed by using atomic absorption spectroscopy.

X-ray Absorption Measurements. Cu K-edge X-ray absorption spectra of HuPrP(90-231) were collected in fluorescence mode at the BM30B FAME beamline of the European Synchrotron Radiation Facility.⁵⁸ A 1.5 mM solution of Cu(II)–HuPrP(90-231) in the presence of 20 mM acetate buffer pH 5.5 was used to collect the cupric form of the protein. Sodium ascorbate was added to the solution under nitrogen atmosphere to collect reduced species. All the spectra were collected at 15 K. The storage ring was running in the two-thirds filling mode with a typical current of 170 mA. The monochromator was equipped with a Si (111) double crystal, in which the second crystal was elastically bent to a cylindrical cross section. The energy resolution at the Cu K-edge is 0.5 eV. The X-ray photon beam was vertically focused by a Ni–Pt mirror, and dynamically sagittally focused in the horizontal size. An array detector made of 30 Ge elements of very high purity was used. The spectra were calibrated by assigning the first inflection point of the Cu foil spectrum to 8981 eV. For each sample, 8 spectra were recorded with a 7 s/point collection statistic and averaged. The collection time was 20 min for each XANES spectrum and 45 min for each EXAFS spectrum. No spectral changes were detected during the data collection.

EXAFS Data Analysis. EXAFS data analysis was performed using the GNXAS code, which is based on a theoretical calculation of the X-ray absorption fine structure signal and a subsequent refinement of the structural parameters.^{59,60} In the GNXAS approach, the interpretation of the experimental data is based on the decomposition of the EXAFS $\chi(k)$ signal (defined as the oscillation with respect to the atomic background cross-section normalized to the corresponding K-edge channel cross-section) into a summation over n -body distribution functions $\gamma^{(n)}$, calculated by means of the multiple-scattering (MS) theory. Each signal has been calculated in the muffin-tin approximation using the Hedin–Lundqvist energy dependent exchange and correlation potential model, which includes inelastic loss effects. The theoretical framework of the GNXAS method is detailed in previous publications.^{59,60}

The analysis of the EXAFS spectra of Cu(II)–HuPrP(90-231) and Cu(I)–HuPrP(90-231) was carried out starting from the coordination model suggested by Hasnain et al.⁶¹ In particular, Cu(II) was found to be coordinated to His96, His111, and two additional low Z ligands (oxygen or nitrogen

donors) in the inner shell and to a sulfur-donating ligand, which was assigned to Met109. The final fit included also one close oxygen-donating ligand that was assumed to derive from solvent, although it could also be derived from a protein ligand such as a Gln98. Based on this model, theoretical EXAFS spectra were calculated to include contributions from first shell two-body signals, and three-atom and four-atom configurations associated with the histidine rings. Previous investigations on model compounds have shown that a quantitative EXAFS analysis of systems containing histidine rings requires a proper treatment of MS four-body terms.^{62,63} The model $\chi(k)$ signal is then refined against the experimental data by using a least-squares minimization procedure in which structural and nonstructural parameters are allowed to float. The structural parameters are bond distance (R) and bond variance (σ_R^2) for a two-body signal, the two shorter bond distances, the intervening angle (θ), and the six covariance matrix elements for a three-body signal. The four-body configurations are described by six geometrical parameters, namely, the three bond distances, two intervening angles (θ and ϕ), and the dihedral angle (ψ) defining the spatial orientation of the three bonds. These parameters were allowed to float within a preset range, typically ± 0.05 Å and $\pm 5^\circ$ for distances and angles respectively, around the average Cu–histidine geometry. During the minimization procedures, the magnitudes of the Debye–Waller terms for the imidazole rings were assumed to increase with distance, and imidazole ring atoms at similar distances from the copper ion were assigned the same value. The EXAFS spectra of Cu(II)–HuPrP(90-231, Q212P) and Cu(I)–HuPrP(90-231, Q212P) were analyzed trying out different possible models including either one or two histidine ligands and a sulfur coordinating atom. In all cases two additional nonstructural parameters were minimized, namely, E_0 (core ionization threshold) and S_0^2 (many body amplitude reduction factor). The quality of the fits was determined by the goodness-of-fit parameters, R_p ,⁶⁰ and by careful inspection of the EXAFS residuals and their Fourier transforms.

XANES Data Analysis. XANES data analysis was carried out with the MXAN code. The X-ray photoabsorption cross section is calculated using the full MS scheme in the framework of the muffin-tin (MT) approximation for the shape of the potential. All details on the potential calculations can be found in ref 64. The real part of the complex exchange and correlation energy is calculated by using the Hedin–Lundqvist (HL) energy-dependent potential. Inelastic processes are accounted for by convolution with a broadening Lorentzian function having an energy-dependent width of the form $\Gamma(E) = \Gamma_c + \Gamma_{\text{mfp}}(E)$. The constant part Γ_c accounts for the core-hole lifetime, and it is fixed to the tabulated value of 1.55 eV fwhm, while the energy-dependent term $\Gamma_{\text{mfp}}(E)$ represents all the intrinsic and extrinsic inelastic processes. Atomic MT radii are calculated based on the Norman criterion including overlap between MT spheres that is optimized by fitting the $ovlp$ parameter (only one parameter for the entire set of MT radii). Another parameter is $V_{0\text{imp}}$, i.e., the value of the muffin-tin potential (V_0) when $ovlp$ is refined to best-fit the model compounds. The potential generator of MXAN (program VGEN) calculates this parameter automatically, and $ovlp$ is the only free parameter of the MS theory with the MT approximation. However, according to this set of calculations, refining also $V_{0\text{imp}}$ improves both the fit and the accuracy of structural results.

Least-squares fits of the XANES experimental data were performed by minimizing the χ^2 function defined as

$$\chi^2 = \frac{1}{me^2} \sum_{i=1}^m [(y_i^{\text{th}} - y_i^{\text{exp}})\varepsilon_i^{-1}]^2 \quad (1)$$

where m is the number of experimental points, and y_i^{th} and y_i^{exp} are the theoretical and experimental values of the absorption cross section; the error ε_i is constant and equal to 0.5% of the experimental jump. Minimization of the χ^2 function was performed in the space of four structural parameters for the WT protein: the Cu–N_{His} distance; the Cu–O/N distance; the Cu–O_{water} distance; and the Cu–S distance. The whole histidine molecules were included, and they were treated as perfectly rigid bodies. In the case of the mutant, different models were tried out to get the best-fit model. A k -weight fitting procedure was followed in all the XANES analysis.

RESULTS

X-ray Absorption Spectra of Cu(II)–HuPrP(90-231) and Cu(I)–HuPrP(90-231). Copper coordination in WT HuPrP(90-231) was investigated by X-ray absorption spectroscopy. Cu(II)–HuPrP(90-231) and Cu(I)–HuPrP(90-231) X-ray absorption spectra revealed changes in the edge energy and shape related to the different copper oxidation states (Figure 2a). A shift of 2–3 eV toward higher energies of the main transition threshold was observed. This is consistent with

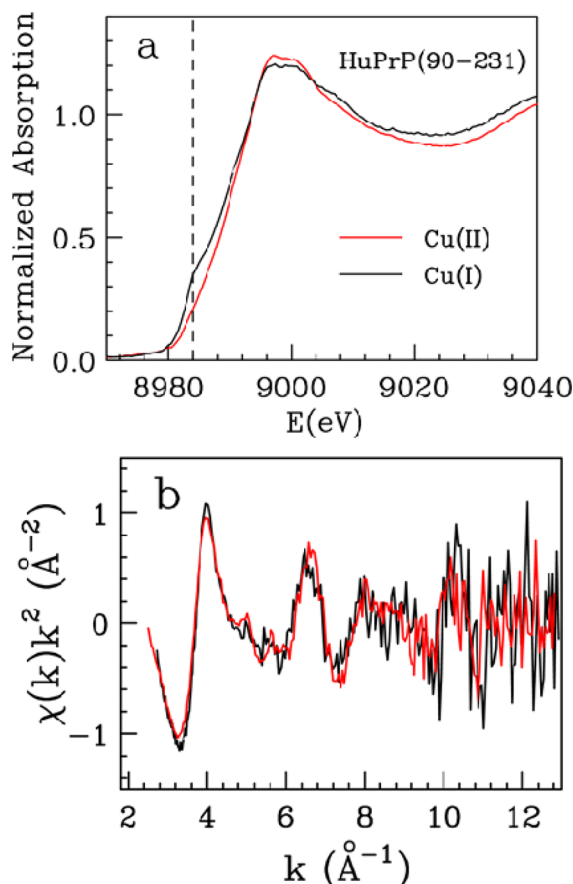


Figure 2. (a) Cu K-edge XANES spectra for Cu(II)–HuPrP(90-231) (red line) and Cu(I)–HuPrP(90-231) (black line). (b) Cu K-edge k^2 -weighted EXAFS data of Cu(II)–HuPrP(90-231) (red line) and Cu(I)–HuPrP(90-231) (black line).

results obtained using model complexes.^{65–67} The pre-edge feature at 8984 eV, assigned to a $1s \rightarrow 4p_z$ transition,⁶⁵ is present in the Cu(I) absorption spectra, but not in those containing Cu(II). The XANES spectrum of Cu(II)–HuPrP(90-231) shown in Figure 2a is very similar to that previously collected at pH 8 published by Hasnain et al.⁶¹ Since we recorded XANES spectra at pH 5.5, this similarity indicates that the Cu(II) binding structure of HuPrP(90-231) is pH-insensitive. This result suggests that, even in the presence of coordinated histidines, no change in the protonation degree occurs for such ligands. Experimental EXAFS data of Cu(II)– and Cu(I)–HuPrP(90-231) extracted with a three-segmented cubic spline are compared in Figure 2b. These two spectra are almost identical, thus indicating that the coordination environment of copper in HuPrP(90-231) is the same despite its oxidation state. Moreover, as already observed for the XANES data, both EXAFS spectra show close resemblance to the data previously collected on Cu(II)–PrP(91-231) at pH = 8.⁶¹ Given the similarity of the experimental data, the quantitative EXAFS analysis of Cu(II)– and Cu(I)–HuPrP(90-231) was carried out starting from the coordination geometry of ref 61. The results of the fitting procedures applied to the Cu(II)– and Cu(I)–HuPrP(90-231) EXAFS spectra are shown in Figure 3, panels C and D. The fitted theoretical signals match the experimental data quite well, and the structural parameters obtained from GNXAS (see above) are almost identical for the two copper oxidation states. The structural parameters are in agreement with the previous determination,⁶¹ within the reported errors (Table 1). To establish error limits on the structural parameters, a number of selected parameters from the fit results were statistically analyzed using two-dimensional contour plots. This analysis examines correlations among fitting parameters and evaluates statistical errors in the determination of the copper coordination structure. The approach is described in detail in ref 60. Briefly, parameters with highest correlation dominate in the error estimate.

The consistency of the analysis is confirmed by the good agreement between the experimental and theoretical Fourier transform (FT) spectra, calculated in the interval k 2.1–10.0 Å⁻¹ with no phase-shift correction applied (Figure 3E,F). FT of oxidized and reduced samples are similar and both characterized by a first-shell peak centered at 1.5 Å and additional outer shell peaks in the distance range between 2 and 4 Å, which has been reported as indicative of histidine binding to the metal ion.^{67–69} The results of our minimization procedures confirm that in both oxidation states copper is coordinated with His96 and His111 (the Cu–N distance is 1.98(2) Å), with two low Z ligands (either oxygen or nitrogen atoms at 1.98 (1.99) Å) and one sulfur scatterer at longer distance (i.e., 3.25 (3.26) Å). In the final fit, one oxygen atom of the solvent at 2.31 (2.32) Å was included as suggested by Hasnain et al.⁶¹ The additional oxygen improves the quality of the fit (R_i improves by 30%). Therefore, the presence of this ligand can be further confirmed on the basis of our data analysis. Moreover, even though the sulfur atom is at greater distance, its inclusion was found to be essential in order to reproduce both the EXAFS and FT experimental spectra (R_i improves by 25%).

In the second step, we applied the MXAN theoretical procedure to analyze XANES data, as the low- and high-energy portions of the XAS spectrum may have different sensitivities to specific structural parameters, such as bond distances and angles. Panels A and B of Figure 3 display the best fitting theoretical XANES spectra of Cu(II)– and Cu(I)–HuPrP(90-

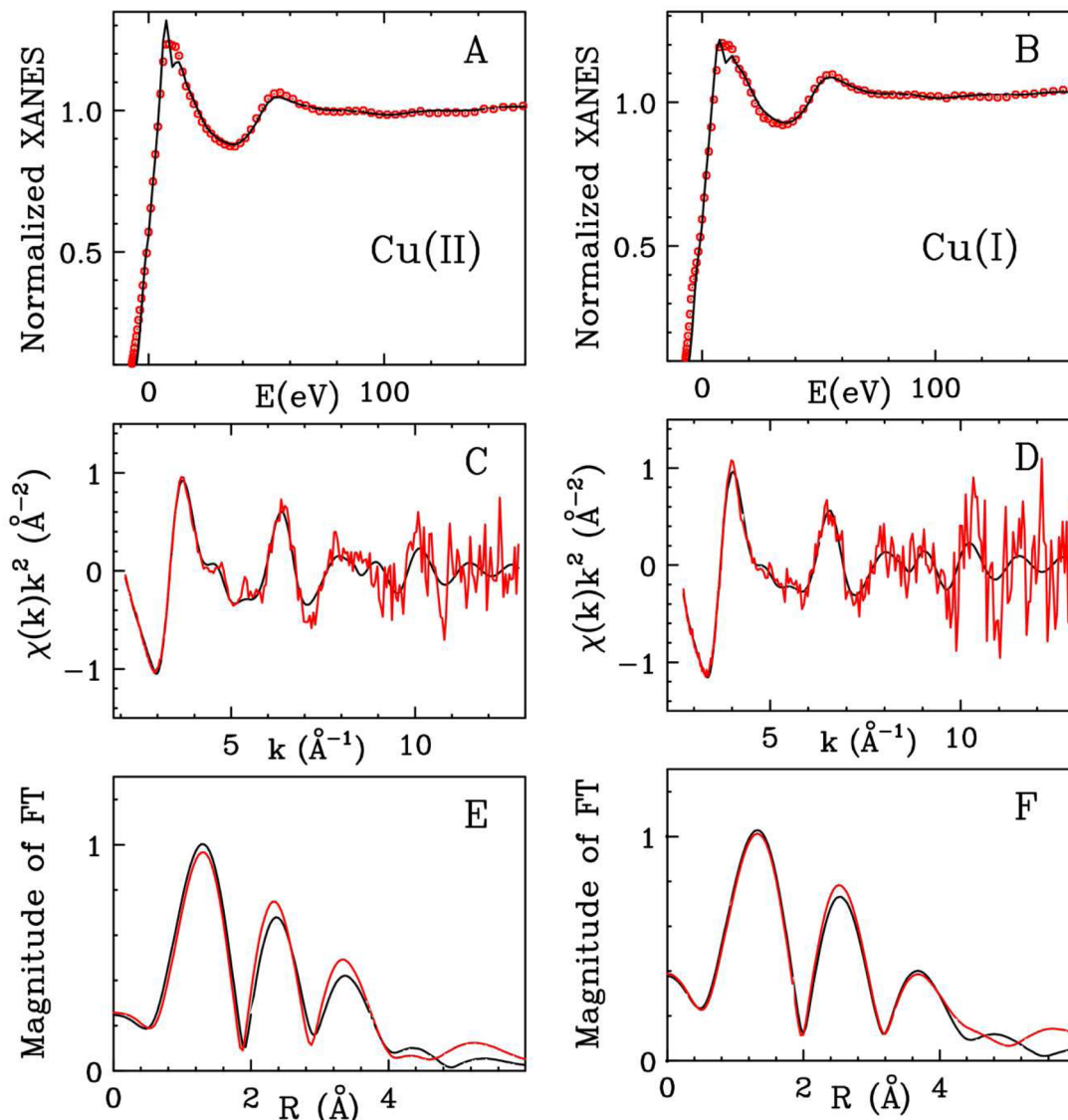


Figure 3. Comparison of the theoretical signal (black line) with experimental data (red line) of Cu K-edge of WT prion protein: XANES data of (A) Cu(II)–HuPrP(90-231) and (B) Cu(I)–HuPrP(90-231); k^2 -weighted EXAFS data of (C) Cu(II)–HuPrP(90-231) and (D) Cu(I)–HuPrP(90-231). Non phase-shift-corrected Fourier transforms of the experimental data (red line) and of the total theoretical signal (black line) of (E) Cu(II)–HuPrP(90-231) and (F) Cu(I)–HuPrP(90-231).

Table 1. Structural Parameters Derived from the EXAFS Analysis of Cu(II)–HuPrP(90-231), Cu(I)–HuPrP(90-231), Cu(II)–HuPrP(90-231, Q212P) and Cu(I)–HuPrP(90-231, Q212P)^a

Cu(II)–HuPrP(90-231)			Cu(I)–HuPrP(90-231)			Cu(II)–HuPrP(90-231, Q212P)			Cu(I)–HuPrP(90-231, Q212P)		
N	R (Å)	σ^2 (Å ²)	N	R (Å)	σ^2 (Å ²)	N	R (Å)	σ^2 (Å ²)	N	R (Å)	σ^2 (Å ²)
2 N _{His}	1.98(2)	0.006(3)	2 N _{His}	1.98(2)	0.006(3)	1 N _{His}	2.00(2)	0.007(3)	1 N _{His}	1.99(2)	0.007(3)
2 O/N	1.98(2)	0.008(3)	2 O/N	1.99(3)	0.009(3)	3 O/N	1.99(2)	0.009(3)	1 O/N	1.99(2)	0.009(3)
1 O	2.31(3)	0.013(4)	1 O	2.32(4)	0.014(4)	1 O	2.40(4)	0.013(4)	1 S	2.28(4)	0.008(3)
1 S	3.25(4)	0.013(4)	1 S	3.26(5)	0.013(4)	1 S	3.47(4)	0.014(4)			

^aN is the coordination number, R is the distance and σ^2 is the Debye–Waller factor. Statistical errors are reported in parentheses.

231), superimposed on the experimental data. The XANES data analysis was carried out starting from the EXAFS geometrical model, and, after optimization, a very good agreement was obtained between the XANES experimental spectrum and theoretical best-fit data (Figure 3A,B). The numerical values of structural parameters extracted by the MXAN optimization procedures for Cu(II)– and Cu(I)–HuPrP(90-231) are compiled in Table 2. Despite the

differences in the edge shape between the XANES spectra of the oxidized and reduced species of the protein, the refined structural parameters obtained by the MXAN analysis are almost identical for Cu(II)– and Cu(I)–HuPrP(90-231), and coincide with the EXAFS determination within statistical errors. The differences observed between the XANES spectra are well reproduced by the MXAN analysis not by structural distortions, but by variation of the broadening function $\Gamma(E)$. Therefore

Table 2. Structural Parameters Derived from the XANES Analysis of Cu(II)–HuPrP(90-231), Cu(I)–HuPrP(90-231), Cu(II)–HuPrP(90-231, Q212P) and Cu(I)–HuPrP(90-231, Q212P)^a

Cu(II)–HuPrP(90-231)		Cu(I)–HuPrP(90-231)		Cu(II)–HuPrP(90-231, Q212P)		Cu(I)–HuPrP(90-231, Q212P)	
N	R (Å)	N	R (Å)	N	R (Å)	N	R (Å)
2 N _{His}	1.92(6)	2 N _{His}	1.91(8)	1 N _{His}	1.91(9)	1 N _{His}	1.91(8)
2 O/N	2.06(4)	2 O/N	2.07(3)	3 O/N	1.98(4)	1 O/N	2.11(3)
1 O	2.26(9)	1 O	2.26(3)	1 O	2.23(9)	1 S	2.19(7)
1 S	3.16(12)	1 S	3.16(12)	1 S	3.14(19)		

^aN is the coordination number, and R is the distance. Statistical errors are reported in parentheses.

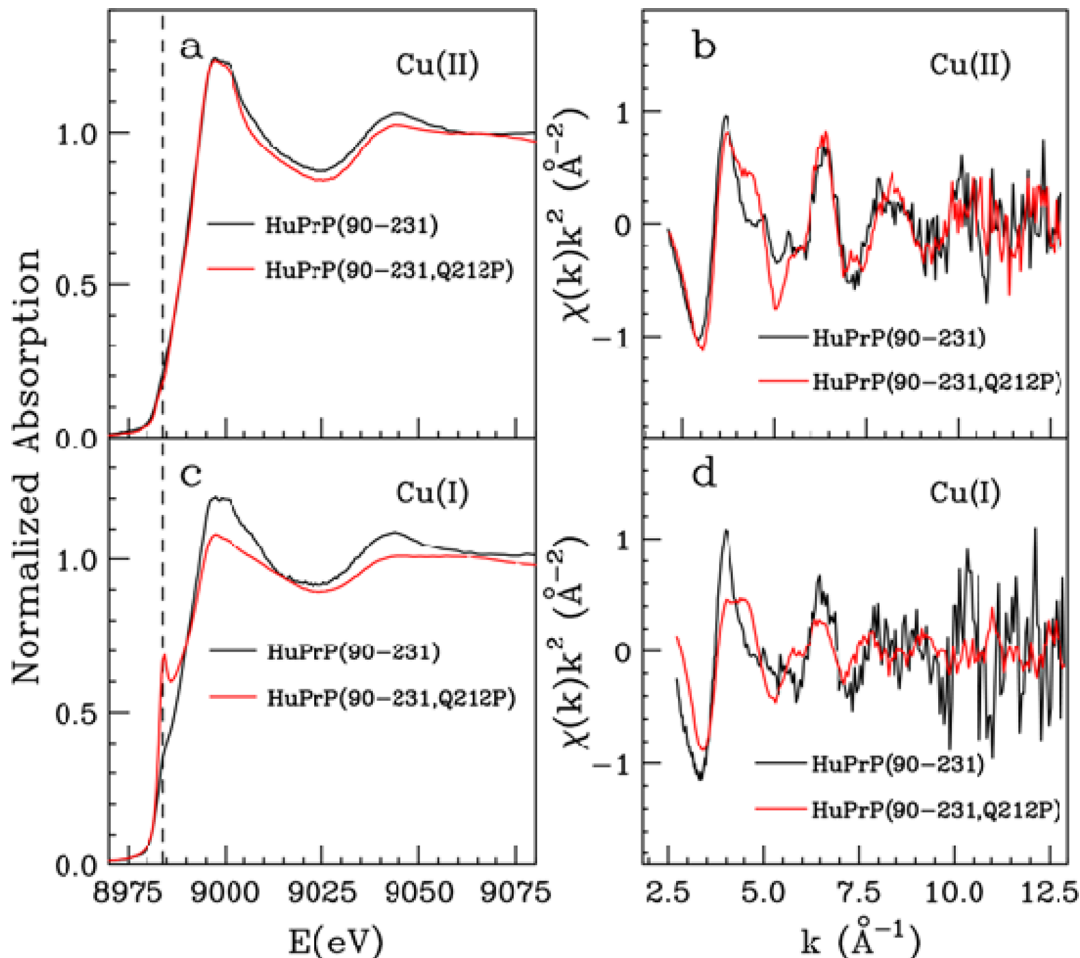


Figure 4. Cu K-edge XANES spectra for (a) Cu(II)–HuPrP(90-231) and Cu(II)–HuPrP(90-231, Q212P) and Cu K-edge k^2 -weighted EXAFS data concerning (b) Cu(II)–HuPrP(90-231) and Cu(II)–HuPrP(90-231, Q212P). Cu K-edge XANES spectra for (c) Cu(I)–HuPrP(90-231) and Cu(I)–HuPrP(90-231, Q212P) and Cu K-edge k^2 -weighted EXAFS data of (d) Cu(I)–HuPrP(90-231) and Cu(I)–HuPrP(90-231, Q212P).

they can be attributed to different electronic configurations within an undistorted metal site in the two oxidation states.

X-ray Absorption Spectra of Cu(II)–HuPrP(90-231, Q212P) and Cu(I)–HuPrP(90-231, Q212P). One of the most interesting findings of the present study concerns copper coordination by HuPrP(90-231, Q212P). Compared to WT, the pathological mutant coordinates Cu(II) and Cu(I) differently. This result is exemplified by the comparison of the XANES and EXAFS spectra of WT HuPrP(90-231) with HuPrP(90-231, Q212P) in the presence of Cu(II) and Cu(I) (Figure 4). The XANES spectrum of Cu(II)–HuPrP(90-231, Q212P) shows differences in the whole energy range as compared to Cu(II)–HuPrP(90-231) (Figure 4a). This result is confirmed by the EXAFS spectra showing markedly different

features in the k range between 3.5 and 4.5 Å⁻¹, which is sensitive to the histidine ligands (Figure 4b). These data indicate that the substitution of a glutamine by a proline at position 212 induces a modification of the Cu(II) binding site in comparison to that present in Cu(II)–HuPrP(90-231).

Much more remarkable changes were found for the Cu(I) ion. Figure 4c,d compares the XANES and EXAFS spectra of Cu(I)–HuPrP(90-231, Q212P) and Cu(I)–HuPrP(90-231). Both XANES spectra display a shoulder at 8984 eV in the rising edge, but this feature is more pronounced in Cu(I)–HuPrP(90-231, Q212P) than in Cu(I)–HuPrP(90-231), suggesting that the coordination environment in the former protein is more centrosymmetric than in the latter (Figure 4c).⁶⁶ The overall shape of XANES spectra differs between the

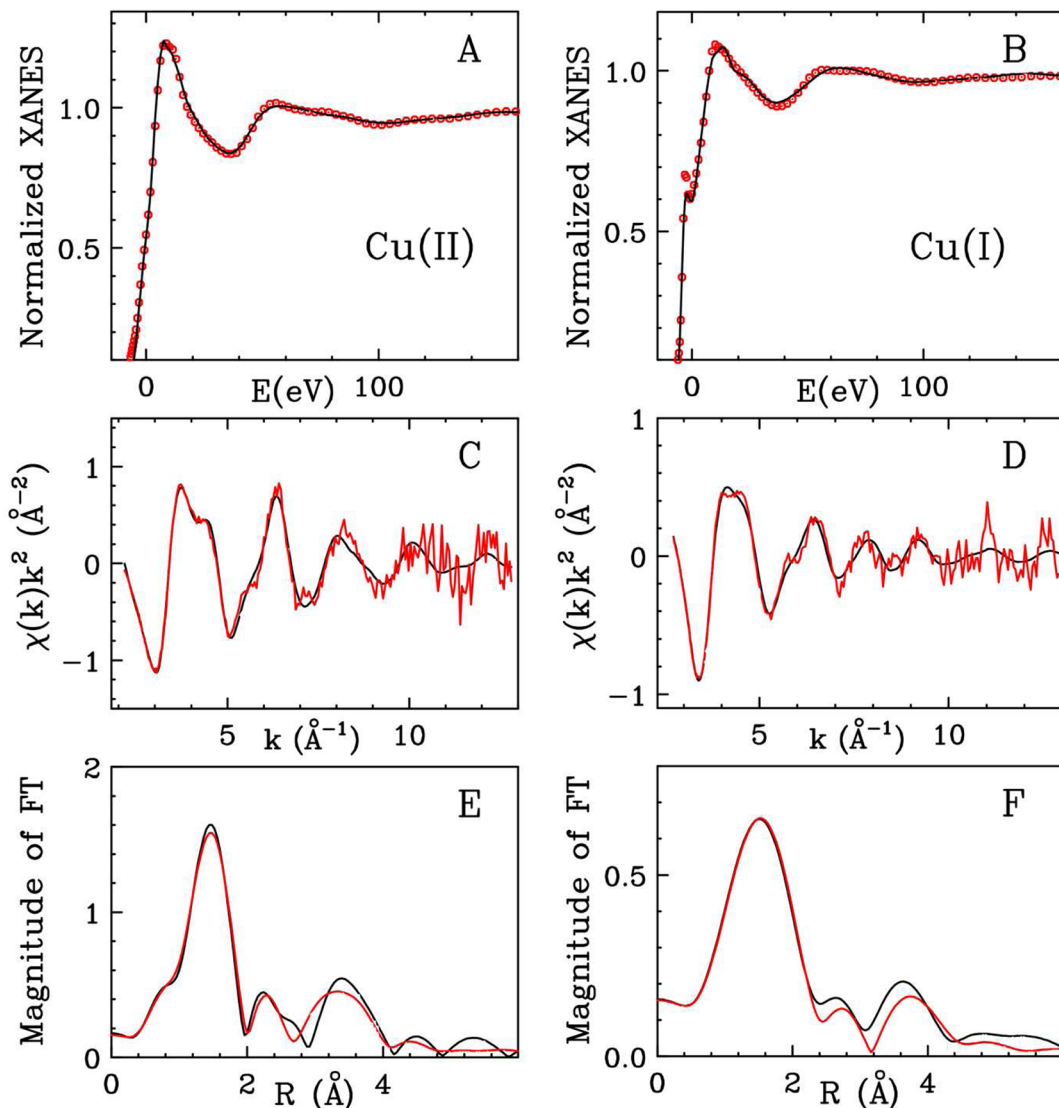


Figure 5. Comparison of the theoretical signal (black line) with experimental data (red line) of Cu K-edge of pathological mutant prion protein: XANES data of (A) Cu(II)–HuPrP(90-231,Q212P) and (B) Cu(I)–HuPrP(90-231,Q212P); k^2 -weighted EXAFS data of (C) Cu(II)–HuPrP(90-231,Q212P) and (D) Cu(I)–HuPrP(90-231,Q212P). Non phase-shift-corrected Fourier transforms of the experimental data (red line) and of the total theoretical signal (black line) of (E) Cu(II)–HuPrP(90-231,Q212P) and (F) Cu(I)–HuPrP(90-231,Q212P).

two proteins, thus highlighting a different coordination geometry of Cu(I) between WT and mutant. EXAFS spectra of Cu(I)–HuPrP(90-231, Q212P) and Cu(I)–HuPrP(90-231) are also altered, confirming differences in copper coordination (Figure 4d).

A deeper insight into the structural modifications of the copper binding site induced by the mutation was gained from the quantitative analysis of EXAFS data of Cu(II)– and Cu(I)–HuPrP(90-231, Q212P). The FT moduli of EXAFS experimental spectra extracted with a three-segmented cubic spline are shown in Figure 5E,F. The FTs were calculated in the interval $k = 2.1\text{--}10.0 \text{ \AA}^{-1}$ with no phase-shift correction applied. The FTs of both Cu(II)– and Cu(I)–HuPrP(90-231, Q212P) are different from the HuPrP(90-231) ones, being characterized by outer shell peaks in the range between 2 and 4 Å with lower amplitude. This may be explained by a single histidine coordinated to the metal ion, thus suggesting that one of the two histidines (namely, His96 and His111) moves away from the metal upon mutation at position 212. The FT first peak width for Cu(I)–HuPrP(90-231, Q212P) is larger than

those of all other examined spectra. This feature may be explained by the presence of sulfur atom(s) entering the Cu(I) first coordination shell, as previously found in other systems.⁶⁷ EXAFS analyses of Cu(II)– and Cu(I)–HuPrP(90-231, Q212P) support a differential coordination environment compared to WT. The best fits for Cu(II)– and Cu(I) mutant are shown in Figure 5C,D (black lines). EXAFS data concerning Cu(II)–HuPrP(90-231, Q212P) could be modeled as a four coordinate copper center with one histidine at 2.00(2) Å, three N/O scatterers at 1.99(2) Å and one more distant sulfur scatterer at 3.47(4) Å. Also in this case, the addition of one oxygen atom at 2.40(3) Å produced a significant improvement of the fit (R_i improves by 30%). Decreasing of coordinated histidine ligands from 2 to 1 is consistent with the reduction in amplitude of the FT higher distance peaks. The geometrical model obtained from the EXAFS analysis has been used as a starter to fit the XANES spectrum, and the results of the MXAN minimization procedure are shown in Figure 5A. The excellent agreement between the experimental and theoretical XANES spectra confirms the validity of the overall

results. The refined structural parameters obtained from the MXAN minimization for Cu(II)–HuPrP(90-231, Q212P) are substantially in agreement with the EXAFS analysis within statistical errors and are listed in Table 2.

The EXAFS analysis of the Cu(I)–HuPrP(90-231, Q212P) protein revealed a 3-fold (or 4-fold) coordination with one histidine at 1.99(2) Å, one N/O scatterer at 1.99(2) Å and 1 (or 2) sulfur scatterers at 2.28(4) Å. It was not possible to establish the number of sulfur atoms present in the Cu(I) first coordination shell on the basis of the EXAFS minimization, as the two models resulted to be in equivalent agreement with the experimental data. However, the three-coordinate model is more reliable considering the presence of the sharp peak at 8984 eV in the rising edge of Cu(I)–HuPrP(90-231, Q212P).

The MXAN analysis of the XANES spectrum for the Cu(I)–HuPrP(90-231, Q212P) mutant aimed at solving the ambiguities found in the EXAFS results on the Cu(I) coordination. A 4-fold coordination model was initially considered, in a square-planar symmetry, including 1 histidine nitrogen, 1 water oxygen, and 2 methionine sulfurs. All the atoms from protein residues were included in the calculations as perfectly rigid bodies. Two different fit strategies were compared: in one, the two methionine sulfur distances were restrained as a single parameter, whereas in the other the two distances were varied independently. Moreover, a single free angular parameter was acting as conformational coordinate of an overall distortion of the copper coordination sphere from square-planar to tetrahedral symmetry. As a result, according to both minimization strategies, the fitting structures have an almost planar symmetry (i.e., the distortion from the perfect planarity along the angular conformational coordinate is always less than 20°). The final best fit is obtained applying the second strategy, by increasing one Cu–S distance of about 0.8 Å. Placing this sulfur away from the Cu coordination sphere resulted in a planar, 3-fold coordination with one histidine nitrogen at 1.91(8) Å, one methionine sulfur at 2.19(7) Å and one oxygen atom of a water molecule at 2.11(3) Å. There is a 0.1 Å discrepancy, larger than the statistical errors, between the two latter values and those obtained by EXAFS. This result could be due either to small systematic errors occasionally present in the MXAN analysis, owing to the well-known MT potential approximations, when applied to open systems with low coordination,^{63,70} or to the neglect of the configurational disorder of the protein.⁵⁴ Notwithstanding these small discrepancies, joining the EXAFS and XANES analyses allowed us to converge on a unique, consistent structural model of Cu(I) coordination within the pathological mutant, clearly distinct from that found for the WT protein.

■ DISCUSSION

The PrP^C interacts with metal ions, particularly copper and zinc. The physiological implication of this interaction is still unclear, as is the role of transition metals in the conversion. Some inconsistencies are reported in the literature regarding the structure and pH dependence of the fifth copper binding site of PrP^C. This site is located in the highly fibrillogenic and toxic region PrP106-126 whose aggregation and neurotoxic properties have been shown to be modulated by divalent cations.^{46,47} Several works hypothesized that peptide fragments are good models for the Cu(II) binding to full-length PrP^C.^{14,71} Therefore, different peptide fragments have been used in EPR, visible CD and EXAFS investigations. Results are nevertheless contradictory, and a unified picture of the fifth copper binding

site structure has not yet emerged. In particular, the experimental EXAFS spectrum of Cu(II)–HuPrP(91-231) collected by Hasnain et al.⁶¹ is markedly different from the experimental EXAFS data reported for the Cu(II)–PrP(91-126) peptide fragment in ref 71. Also, the EXAFS quantitative analysis of the two spectra produced different coordination environments for the Cu(II) ion and these conflicting results were ascribed to the different pH values used in the experiments. Since the conversion from PrP^C to PrP^{Sc} seems to occur in the acidic endosomal compartments,^{69,71,72} we performed our measurements at pH 5.5. The EXAFS experimental spectrum of the Cu(II)–HuPrP(90-231) complex at pH 5.5 shown in Figure 2b strongly resembles that previously obtained by Hasnain et al.⁶¹ on HuPrP(91-231) at pH 8, indicating that the Cu(II) binding structure is pH-insensitive. As a consequence, the differences of the EXAFS spectra and, accordingly, of the Cu(II) binding site between the non-OR PrP^C and the peptide PrP(91-126) are not due to the different pH but very likely to the fact that peptide fragments cannot be used as models for the full-length protein. This finding suggests that the non-OR copper-binding site interacts with the globular domain. This has been shown by Thakur et al.,⁷³ who reported that the region 90–120, containing the binding site His96/His111, becomes proximal to the α_1 -helix for interaction upon copper binding.⁷³ To evaluate the effect of this complex network of interactions on the His96/His111 copper-binding site, structural studies should be performed on the entire C-terminal domain and not on short peptides. As shown in Figure 2b, the EXAFS spectra of Cu(II)–HuPrP(90-231) and Cu(I)–HuPrP(90-231) are identical, indicating that the copper binding site is the same despite its oxidation state.

Also the structural parameters obtained from the quantitative analysis of the EXAFS and XANES are equal for Cu(II) and Cu(I) within the reported errors (see Table 1). These analyses revealed that His residues 96 and 111 are involved in binding both Cu(II) and Cu(I) in conjunction with at least two extra coordinating groups. Based on our data, we prepared three putative models of Cu(II) and Cu(I) that are bound to the WT and to the mutant protein employing bond lengths derived from the XAFS analysis (Figure 6). The preservation of the copper structural environment is of note and brings about an interesting, unexpected result. Previously it has been shown that Cu(II) and Cu(I) are preferentially chelated by histidine-rich and methionine-rich peptides, respectively.⁶⁷ This peculiarity could facilitate the redox cycling reversibility for a not-yet-identified physiological function.

In addition, we studied the effect of the pathological point mutation Q212P on the structure of the fifth copper-binding site. NMR structure of HuPrP(90-231, Q212P) revealed unique features such as the breakage of α_3 -helix between Glu200 and Tyr226 with subsequent changes of hydrophobic interactions with β_2 – α_2 loop region. In the mutant, this loop is characterized by the exposure of aromatic residues Tyr163, Tyr169 and Phe175.⁴¹ Both XANES and EXAFS spectra of Cu(II)–HuPrP(90-231, Q212P) are different from those of the WT protein (see Figures 4a and 4b). This result highlights a dramatic modification of the Cu(II) fifth binding site caused by the pathological point mutation in the globular domain. This finding reinforces the hypothesis that the structure of the His96/His111 binding site is strongly influenced by the interactions between the globular domain and the N-terminal tail, though these interactions have not been observed by NMR spectroscopy because of high flexibility of the tail. Therefore,

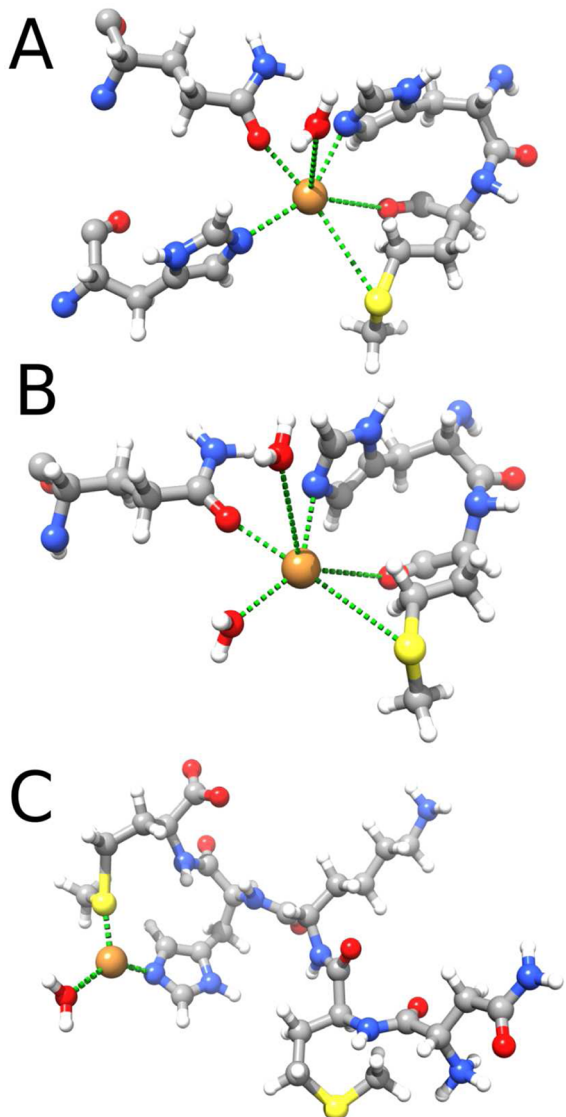


Figure 6. Schematic representations of copper binding sites in (A) Cu(II)–HuPrP(90–231) and Cu(I)–HuPrP(90–231), (B) Cu(II)–HuPrP(90–231, Q212P) and (C) Cu(I)–HuPrP(90–231, Q212P) complexes. Blue spheres identify nitrogen atoms, red spheres are oxygen atoms and yellow spheres encode for sulfur atoms. Gray and white spheres represent carbon and hydrogen atoms respectively.

short peptide fragments are not able to mimic both C-terminal domain and full-length protein. The analysis of the EXAFS and XANES spectra of Cu(II)–HuPrP(90–231, Q212P) revealed that in the mutant the Cu(II) ion is coordinated by a single histidine, suggesting that either His96 or His111 moves away from the metal (Figure 6B). The increased flexibility of the globular domain in Q212P mutant results in a less structured Cu(II) fifth binding site that becomes very similar to the coordination adopted by the Cu(II) ion in the PrP(91–126) peptide.⁷¹

As illustrated in Figures 4c and 4d, XANES and EXAFS spectra of the Cu(I)–HuPrP(90–231, Q212P) complex are very different from those of the WT protein, showing that the mutation modifies the fifth binding site not only for the cupric complex but also for the reduced one. Also in this case, EXAFS and XANES data analyses indicate that Cu(I) ion is coordinated by a single histidine but, unlike all other metal–

protein complexes, sulfur atoms and thus methionine residues enter the first coordination shell at quite a short distance (2.28(4) Å) (Figure 6C). Interestingly, copper-binding sites in the mutant resemble those obtained using peptides, confirming the loss of short- and long-range interactions.^{41–43} While in the WT protein the copper-binding site has the same structure for both Cu(II) and Cu(I), in the case of the mutant protein the coordination site changes drastically from the oxidized to the reduced form of the copper ion. This finding could have important implications on the redox activity of the protein.

Despite numerous endeavors in the prion field, the molecular mechanisms of the conversion remain enigmatic. Pathological point mutations and their structure-related changes may help to disclose these molecular mechanisms. Main structural features such as the disorder β_2 – α_2 loop, the increased distance between this loop and α_3 helix and the subsequent exposure of hydrophobic residues to solvent have been associated with some mutants.^{41–43} Nevertheless, the mutants fold mainly in α -helices.^{74–77} The propensity of mutants to convert into β -sheet enriched aggregates has been extensively studied as a function of thermodynamic destabilization.^{33–36} These data suggest that thermodynamic destabilization of mutants is not the basis of disease phenotype in familial human TSEs. Other molecular mechanisms such as altered metal-binding and oxidative stress are required for the conversion.

In the present work, we highlighted changes in copper coordination induced by the point mutation Q212P, in both oxidation states. Unlike WT, the mutant behaves as peptide studies have shown, probably causing alterations in copper homeostasis and, therefore, in redox control. Different modes of Cu-coordination result in the formation of stable β -hairpin structures in the non-OR Cu-binding region. These hairpins have been postulated to initiate misfolding through interactions with the C-terminal part of PrP, especially in the region 90–120 that partially overlaps with the well-established amyloidogenic stretch 106–126. These hairpins may also yield more stable β -sheet structures that might associate in the same fashion with additional PrP.^{73,78} The pathological implications of these alterations might also include metal-induced oxidative damage, and in some instances conversion of the cellular form into PrP^{Sc}. Recently, Canello et al.⁷⁹ showed that fibroblasts generated from both PrP-ablated mice and a transgenic mouse line mimicking E200K-caused CJD were significantly more sensitive to copper toxicity than WT PrP containing fibroblasts.⁷⁹ This provides important evidence that the proper PrP^C fold is required to manage copper ions and then to protect cells from oxidative stress. These data corroborate the hypothesis that disease-linked mutations may have a structural effect both on the globular domain and on the N-terminal part where functional domains are present. Our findings suggest that the structural modifications observed in the mutant PrP point out to a well-defined structure–function relationship for the understanding of spontaneous generation of PrP^{Sc} in inherited prion diseases.

AUTHOR INFORMATION

Corresponding Author

*P.D'A.: tel, +39-06-49913751; e-mail, p.dangelo@caspur.it.
F.B.: tel, +39-0425-377512; e-mail, federico.benetti@venetonanotech.it.

Present Address

▽ ECSIN-European Center for the Sustainable Impact of Nanotechnology, Veneto Nanotech S.C.p.A., I-45100 Rovigo, Italy.

Funding

This work was supported by CASPUR with the Standard HPC Grant 2012 entitled, “A combined X-ray absorption spectroscopy, Molecular Dynamics simulations and Quantum Mechanics calculation procedure for the structural characterization of ill-defined systems”; and by a PRIN 2008 grant entitled, “Produzione e caratterizzazione strutturale e biologica di isomeri conformazionali della proteina prionica”.

Notes

The authors declare no competing financial interest.

ACKNOWLEDGMENTS

We acknowledge the European Synchrotron Radiation Facility and the staff of BM30B for their helpful support.

ABBREVIATIONS USED

TSEs, transmissible spongiform encephalopathies; PrP^C, cellular prion protein; PrP^{Sc}, prion; XAFS, X-ray absorption fine structure; EXAFS, extended X-ray absorption fine structure; XANES, X-ray absorption near-edge structure; WT HuPrP(90-231), C-terminal domain of wild-type human prion protein; HuPrP(90-231, Q212P), C-terminal domain of human prion protein carrying the pathological mutation Q212P

REFERENCES

- (1) Zahn, R., Liu, A., Luhrs, T., Riek, R., von Schroetter, C., Lopez Garcia, F., Billeter, M., Calzolai, L., Wider, G., and Wuthrich, K. (2000) NMR solution structure of the human prion protein. *Proc. Natl. Acad. Sci. U.S.A.* 97, 145–150.
- (2) Pan, K. M., Stahl, N., and Prusiner, S. B. (1992) Purification and properties of the cellular prion protein from Syrian hamster brain. *Protein Sci.* 1, 1343–1352.
- (3) Hornshaw, M. P., McDermott, J. R., and Candy, J. M. (1995) Copper binding to the N-terminal tandem repeat regions of mammalian and avian prion protein. *Biochem. Biophys. Res. Commun.* 207, 621–629.
- (4) Hornshaw, M. P., McDermott, J. R., Candy, J. M., and Lakey, J. H. (1995) Copper binding to the N-terminal tandem repeat region of mammalian and avian prion protein: structural studies using synthetic peptides. *Biochem. Biophys. Res. Commun.* 214, 993–999.
- (5) Brown, D. R., Hafiz, F., Glasssmith, L. L., Wong, B. S., Jones, I. M., Clive, C., and Haswell, S. J. (2000) Consequences of manganese replacement of copper for prion protein function and proteinase resistance. *EMBO J.* 19, 1180–1186.
- (6) Jackson, G. S., Murray, I., Hosszu, L. L., Gibbs, N., Waltho, J. P., Clarke, A. R., and Collinge, J. (2001) Location and properties of metal-binding sites on the human prion protein. *Proc. Natl. Acad. Sci. U.S.A.* 98, 8531–8535.
- (7) Jones, C. E., Klewpatinond, M., Abdelraheim, S. R., Brown, D. R., and Viles, J. H. (2005) Probing copper²⁺ binding to the prion protein using diamagnetic nickel²⁺ and ¹H NMR: the unstructured N terminus facilitates the coordination of six copper²⁺ ions at physiological concentrations. *J. Mol. Biol.* 346, 1393–1407.
- (8) Singh, N., Das, D., Singh, A., and Mohan, M. L. (2010) Prion protein and metal interaction: physiological and pathological implications. *Curr. Issues Mol. Biol.* 12, 99–107.
- (9) Chattopadhyay, M., Walter, E. D., Newell, D. J., Jackson, P. J., Aronoff-Spencer, E., Peisach, J., Gerfen, G. J., Bennett, B., Antholine, W. E., and Millhauser, G. L. (2005) The octarepeat domain of the prion protein binds Cu(II) with three distinct coordination modes at pH 7.4. *J. Am. Chem. Soc.* 127, 12647–12656.
- (10) Liu, L., Jiang, D., McDonald, A., Hao, Y., Millhauser, G. L., and Zhou, F. (2011) Copper redox cycling in the prion protein depends critically on binding mode. *J. Am. Chem. Soc.* 133, 12229–12237.
- (11) Whittal, R. M., Ball, H. L., Cohen, F. E., Burlingame, A. L., Prusiner, S. B., and Baldwin, M. A. (2000) Copper binding to octarepeat peptides of the prion protein monitored by mass spectrometry. *Protein Sci.* 9, 332–343.
- (12) Kramer, M. L., Kratzin, H. D., Schmidt, B., Romer, A., Windl, O., Liemann, S., Hornemann, S., and Kretzschmar, H. (2001) Prion protein binds copper within the physiological concentration range. *J. Biol. Chem.* 276, 16711–16719.
- (13) Millhauser, G. L. (2007) Copper and the prion protein: methods, structures, function, and disease. *Annu. Rev. Phys. Chem.* 58, 299–320.
- (14) Jones, C. E., Abdelraheim, S. R., Brown, D. R., and Viles, J. H. (2004) Preferential Cu²⁺ coordination by His96 and His111 induces beta-sheet formation in the unstructured amyloidogenic region of the prion protein. *J. Biol. Chem.* 279, 32018–32027.
- (15) Younan, N. D., Klewpatinond, M., Davies, P., Ruban, A. V., Brown, D. R., and Viles, J. H. (2011) Copper(II)-induced secondary structure changes and reduced folding stability of the prion protein. *J. Mol. Biol.* 410, 369–382.
- (16) Wong, B. S., Liu, T., Li, R., Pan, T., Petersen, R. B., Smith, M. A., Gambetti, P., Perry, G., Manson, J. C., Brown, D. R., and Sy, M. S. (2001) Increased levels of oxidative stress markers detected in the brains of mice devoid of prion protein. *J. Neurochem.* 76, 565–572.
- (17) Vassallo, N., and Herms, J. (2003) Cellular prion protein function in copper homeostasis and redox signalling at the synapse. *J. Neurochem.* 86, 538–544.
- (18) Chen, S., Mange, A., Dong, L., Lehmann, S., and Schachner, M. (2003) Prion protein as trans-interacting partner for neurons is involved in neurite outgrowth and neuronal survival. *Mol. Cell. Neurosci.* 22, 227–233.
- (19) Kanaani, J., Prusiner, S. B., Diacovo, J., Baekkeskov, S., and Legname, G. (2005) Recombinant prion protein induces rapid polarization and development of synapses in embryonic rat hippocampal neurons in vitro. *J. Neurochem.* 95, 1373–1386.
- (20) Santuccione, A., Sytnyk, V., Leshchyns'ka, I., and Schachner, M. (2005) Prion protein recruits its neuronal receptor NCAM to lipid rafts to activate p59fyn and to enhance neurite outgrowth. *J. Cell Biol.* 169, 341–354.
- (21) Aguzzi, A., Baumann, F., and Bremer, J. (2008) The prion's elusive reason for being. *Annu. Rev. Neurosci.* 31, 439–477.
- (22) Brown, D. R. (2003) Prion protein expression modulates neuronal copper content. *J. Neurochem.* 87, 377–385.
- (23) Kralovicova, S., Fontaine, S. N., Alderton, A., Alderman, J., Ragnarsdottir, K. V., Collins, S. J., and Brown, D. R. (2009) The effects of prion protein expression on metal metabolism. *Mol. Cell. Neurosci.* 41, 135–147.
- (24) Pushie, M. J., Pickering, I. J., Martin, G. R., Tsutsui, S., Jirik, F. R., and George, G. N. (2011) Prion protein expression level alters regional copper, iron and zinc content in the mouse brain. *Metalomics* 3, 206–214.
- (25) Roucou, X., and LeBlanc, A. C. (2005) Cellular prion protein neuroprotective function: implications in prion diseases. *J. Mol. Med. (Berlin)* 83, 3–11.
- (26) Prusiner, S. B. (1998) Prions. *Proc. Natl. Acad. Sci. U.S.A.* 95, 13363–13383.
- (27) Benetti, F., and Legname, G. (2009) De novo mammalian prion synthesis. *Prion* 3, 213–219.
- (28) Hill, A. F., Antoniou, M., and Collinge, J. (1999) Protease-resistant prion protein produced in vitro lacks detectable infectivity. *J. Gen. Virol.* 80 (Part 1), 11–14.
- (29) Cohen, F. E., and Prusiner, S. B. (1998) Pathologic conformations of prion proteins. *Annu. Rev. Biochem.* 67, 793–819.
- (30) Legname, G., Giachin, G., and Benetti, F. (2012) *Structural Studies of Prion Proteins and Prions Non-fibrillar Amyloidogenic Protein Assemblies—Common Cytotoxins Underlying Degenerative Diseases* (Rahimi, F., Bitan, G., Eds.) pp 289–317, Springer, The Netherlands.

- (31) Requena, J. R. (2009) Structure of mammalian prions. *Future Virol.* 4, 295–307.
- (32) van der Kamp, M. W., and Daggett, V. (2009) The consequences of pathogenic mutations to the human prion protein. *Protein Eng. Des. Sel.* 22, 461–468.
- (33) Apetri, A. C., Surewicz, K., and Surewicz, W. K. (2004) The effect of disease-associated mutations on the folding pathway of human prion protein. *J. Biol. Chem.* 279, 18008–18014.
- (34) Liemann, S., and Glockshuber, R. (1999) Influence of amino acid substitutions related to inherited human prion diseases on the thermodynamic stability of the cellular prion protein. *Biochemistry* 38, 3258–3267.
- (35) Vanik, D. L., and Surewicz, W. K. (2002) Disease-associated F198S mutation increases the propensity of the recombinant prion protein for conformational conversion to scrapie-like form. *J. Biol. Chem.* 277, 49065–49070.
- (36) Swietnicki, W., Petersen, R. B., Gambetti, P., and Surewicz, W. K. (1998) Familial mutations and the thermodynamic stability of the recombinant human prion protein. *J. Biol. Chem.* 273, 31048–31052.
- (37) Ashok, A., and Hegde, R. S. (2009) Selective processing and metabolism of disease-causing mutant prion proteins. *PLoS Pathog.* 5, e1000479.
- (38) Hegde, R. S., Mastrianni, J. A., Scott, M. R., DeFea, K. A., Tremblay, P., Torchia, M., DeArmond, S. J., Prusiner, S. B., and Lingappa, V. R. (1998) A transmembrane form of the prion protein in neurodegenerative disease. *Science* 279, 827–834.
- (39) Heske, J., Heller, U., Winklhofer, K. F., and Tatzelt, J. (2004) The C-terminal globular domain of the prion protein is necessary and sufficient for import into the endoplasmic reticulum. *J. Biol. Chem.* 279, 5435–5443.
- (40) Mishra, R. S., Bose, S., Gu, Y., Li, R., and Singh, N. (2003) Aggresome formation by mutant prion proteins: the unfolding role of proteasomes in familial prion disorders. *J. Alzheimer's Dis.* 5, 15–23.
- (41) Ilc, G., Giachin, G., Jaremko, M., Jaremko, L., Benetti, F., Plavec, J., Zhukov, I., and Legname, G. (2010) NMR structure of the human prion protein with the pathological Q212P mutation reveals unique structural features. *PLoS One* 5, e11715.
- (42) Biljan, I., Ilc, G., Giachin, G., Raspadori, A., Zhukov, I., Plavec, J., and Legname, G. (2011) Toward the Molecular Basis of Inherited Prion Diseases: NMR Structure of the Human Prion Protein with V210I Mutation. *J. Mol. Biol.* 412 (4), 660–673.
- (43) Rossetti, G., Cong, X., Caliandro, R., Legname, G., and Carloni, P. (2011) Common Structural Traits across Pathogenic Mutants of the Human Prion Protein and Their Implications for Familial Prion Diseases. *J. Mol. Biol.* 411, 700–712.
- (44) Yin, S., Pham, N., Yu, S., Li, C., Wong, P., Chang, B., Kang, S. C., Biasini, E., Tien, P., Harris, D. A., and Sy, M. S. (2007) Human prion proteins with pathogenic mutations share common conformational changes resulting in enhanced binding to glycosaminoglycans. *Proc. Natl. Acad. Sci. U.S.A.* 104, 7546–7551.
- (45) Singh, N., Singh, A., Das, D., and Mohan, M. L. (2010) Redox control of prion and disease pathogenesis. *Antioxid. Redox Signaling* 12, 1271–1294.
- (46) Wang, Y., Xu, J., Wang, L., Zhang, B., and Du, W. (2010) Interaction of the human prion protein PrP106-126 with metal complexes: potential therapeutic agents against prion disease. *Chemistry* 16, 13339–13342.
- (47) Jobling, M. F., Huang, X., Stewart, L. R., Barnham, K. J., Curtain, C., Volitakis, I., Perugini, M., White, A. R., Cherny, R. A., Masters, C. L., Barrow, C. J., Collins, S. J., Bush, A. I., and Cappai, R. (2001) Copper and zinc binding modulates the aggregation and neurotoxic properties of the prion peptide PrP106-126. *Biochemistry* 40, 8073–8084.
- (48) Kovacs, G. G., Trabattoni, G., Hainfellner, J. A., Ironside, J. W., Knight, R. S., and Budka, H. (2002) Mutations of the prion protein gene phenotypic spectrum. *J. Neurol.* 249, 1567–1582.
- (49) Beck, J. A., Poulter, M., Campbell, T. A., Adamson, G., Uphill, J. B., Guerreiro, R., Jackson, G. S., Stevens, J. C., Manji, H., Collinge, J., and Mead, S. (2010) PRNP allelic series from 19 years of prion protein gene sequencing at the MRC Prion Unit. *Hum. Mutat.* 31, E1551–E1563.
- (50) Cook, J. D., Penner-Hahn, J. E., and Stemmler, T. L. (2008) Structure and dynamics of metalloproteins in live cells. *Methods Cell Biol.* 90, 199–216.
- (51) Strange, R. W., and Feiters, M. C. (2008) Biological X-ray absorption spectroscopy (BioXAS): a valuable tool for the study of trace elements in the life sciences. *Curr. Opin. Struct. Biol.* 18, 609–616.
- (52) D'Angelo, P., Della Longa, S., Arcovito, A., Anselmi, M., Di Nola, A., and Chillemi, G. (2010) Dynamic investigation of protein metal active sites: interplay of XANES and molecular dynamics simulations. *J. Am. Chem. Soc.* 132, 14901–14909.
- (53) D'Angelo, P., Bottari, E., Festa, M. R., Nolting, H. F., and Pavel, N. V. (1998) X-ray Absorption Study of Copper(II)-Glycinate Complexes in Aqueous Solution. *J. Phys. Chem. B* 102, 3114–3122.
- (54) Lee, P. A., and Pendry, J. B. (1975) Theory of the extended x-ray absorption fine structure. *Phys. Rev. B* 11, 2795–2811.
- (55) Rehr, J. J., and Albers, R. C. (2000) Theoretical approaches to x-ray absorption fine structure. *Rev. Mod. Phys.* 72, 621–654.
- (56) Natoli, C. R., Benfatto, M., Della Longa, S., and Hatada, K. (2003) X-ray absorption spectroscopy: state-of-the-art analysis. *J. Synchrotron Radiat.* 10, 26–42.
- (57) Studier, F. W. (2005) Protein production by auto-induction in high density shaking cultures. *Protein Expression Purif.* 41, 207–234.
- (58) Proux, O., Biquard, X., Lahera, E., Menthonnex, J. J., Prat, A., Ulrich, O., Soldo, Y., Trévisson, P., Kapoujyan, G., Perroux, G., Taunier, P., Grand, D., Jeantet, P., Deleglise, M., Roux, J.-P., and Hazemann, J.-L. (2005) FAME: A New Beamline for X-Ray Absorption Investigations of Very-Diluted Systems of Environmental, Material and Biological Interests. *Phys. Scr. T115*, 970–973.
- (59) Filipponi, A., Di Cicco, A., and Natoli, C. R. (1995) X-ray-absorption spectroscopy and n-body distribution functions in condensed matter. I. Theory. *Phys. Rev. B* 52, 15122–15134.
- (60) Filipponi, A., and Di Cicco, A. (1995) X-ray-absorption spectroscopy and n-body distribution functions in condensed matter. II. Data analysis and applications. *Phys. Rev. B* 52, 15135–15149.
- (61) Hasnain, S. S., Murphy, L. M., Strange, R. W., Grossmann, J. G., Clarke, A. R., Jackson, G. S., and Collinge, J. (2001) XAFS study of the high-affinity copper-binding site of human PrP(91-231) and its low-resolution structure in solution. *J. Mol. Biol.* 311, 467–473.
- (62) Zhang, H. H., Filipponi, A., Di Cicco, A., Scott, M. J., Holm, R. H., Hedman, B., and Hogdson, K. O. (1997) Multiple-Edge XAS Studies of Cyanide-Bridged Iron–Copper Molecular Assemblies Relevant to Cyanide-Inhibited Heme–Copper Oxidases Using Four-Body Multiple-Scattering Analysis. *J. Am. Chem. Soc.* 119, 2470–2478.
- (63) D'Angelo, P., Lapi, A., Migliorati, V., Arcovito, A., Benfatto, M., Roscioni, O. M., Meyer-Klaucke, W., and Della-Longa, S. (2008) X-ray absorption spectroscopy of hemes and hemeproteins in solution: multiple scattering analysis. *Inorg. Chem.* 47, 9905–9918.
- (64) Benfatto, M., and Della Longa, S. (2001) Geometrical fitting of experimental XANES spectra by a full multiple-scattering procedure. *J. Synchrotron Radiat.* 8, 1087–1094.
- (65) Pickering, I. J., George, G. N., Dameron, C. T., Kurz, B., Winge, D. R., and Dance, I. G. (1993) X-ray Absorption Spectroscopy of Cuprous-Thiolate Clusters in Proteins and Model Systems. *J. Am. Chem. Soc.* 115, 9498–9505.
- (66) Kau, L. S., Spira-Solomon, J., Penner-Hahn, J. E., Hogdson, K. O., and Solomon, E. I. (1987) X-ray absorption edge determination of the oxidation state and coordination number of copper. Application to the type 3 site in *Rhus vernicifera* laccase and its reaction with oxygen. *J. Am. Chem. Soc.* 109, 6433–6442.
- (67) D'Angelo, P., Pacello, F., Mancini, G., Proux, O., Hazemann, J. L., Desideri, A., and Battistoni, A. (2005) X-ray absorption investigation of a unique protein domain able to bind both copper(I) and copper(II) at adjacent sites of the N-terminus of Haemophilus ducreyi Cu,Zn superoxide dismutase. *Biochemistry* 44, 13144–13150.

- (68) Pearson, K., Huffman, D. L., Penner-Hahn, J. E., and O'Halloran, T. V. (2003) The PcoC copper resistance protein coordinates Cu(I) via novel S-methionine interactions. *J. Am. Chem. Soc.* **125**, 342–343.
- (69) Arnesano, F., Banci, L., Bertini, I., Mangani, S., and Thompsett, A. R. (2003) A redox switch in CopC: an intriguing copper trafficking protein that binds copper(I) and copper(II) at different sites. *Proc. Natl. Acad. Sci. U.S.A.* **100**, 3814–3819.
- (70) Arcovito, A., Ardiccioni, C., Cianci, M., D'Angelo, P., Vallone, B., and Della Longa, S. (2010) Polarized X-ray absorption near-edge structure spectroscopy of neuroglobin and myoglobin single crystals. *J. Phys. Chem. B* **114**, 13223–13231.
- (71) Shearer, J., and Soh, P. (2007) The copper(II) adduct of the unstructured region of the amyloidogenic fragment derived from the human prion protein is redox-active at physiological pH. *Inorg. Chem.* **46**, 710–719.
- (72) Marijanovic, Z., Caputo, A., Campana, V., and Zurzolo, C. (2009) Identification of an intracellular site of prion conversion. *PLoS Pathog.* **5**, e1000426.
- (73) Thakur, A. K., Srivastava, A. K., Srinivas, V., Chary, K. V., and Rao, C. M. (2011) Copper alters aggregation behavior of prion protein and induces novel interactions between its N- and C-terminal regions. *J. Biol. Chem.* **286**, 38533–38545.
- (74) Calzolai, L., Lysik, D. A., Guntert, P., von Schroetter, C., Riek, R., Zahn, R., and Wuthrich, K. (2000) NMR structures of three single-residue variants of the human prion protein. *Proc. Natl. Acad. Sci. U.S.A.* **97**, 8340–8345.
- (75) Calzolai, L., and Zahn, R. (2003) Influence of pH on NMR structure and stability of the human prion protein globular domain. *J. Biol. Chem.* **278**, 35592–35596.
- (76) Zhang, Y., Swietnicki, W., Zagorski, M. G., Surewicz, W. K., and Sonnichsen, F. D. (2000) Solution structure of the E200K variant of human prion protein. Implications for the mechanism of pathogenesis in familial prion diseases. *J. Biol. Chem.* **275**, 33650–33654.
- (77) Lee, S., Antony, L., Hartmann, R., Knaus, K. J., Surewicz, K., Surewicz, W. K., and Yee, V. C. (2010) Conformational diversity in prion protein variants influences intermolecular beta-sheet formation. *EMBO J.* **29**, 251–262.
- (78) Pushie, M. J., and Vogel, H. J. (2009) A potential mechanism for Cu²⁺ reduction, beta-cleavage, and beta-sheet initiation within the N-terminal domain of the prion protein: insights from density functional theory and molecular dynamics calculations. *J. Toxicol. Environ. Health, A* **72**, 1040–1059.
- (79) Canello, T., Friedman-Levi, Y., Mizrahi, M., Binyamin, O., Cohen, E., Frid, K., and Gabizon, R. (2012) Copper is toxic to PrP-ablated mice and exacerbates disease in a mouse model of E200K genetic prion disease. *Neurobiol. Dis.* **45** (3), 1010–1017.